Validation of High-Throughput Wound Healing Assay using 3D Cell Patterning and Automated, Kinetic Imaging

Brad Larson and Peter Banks, BioTek Instruments, Inc., Winooski, VT
Glauco R. Souza, William Haisler, Nano3D Biosciences, Inc., Houston, TX
Jan Seldin, Greiner Bio-One, Monroe, NC

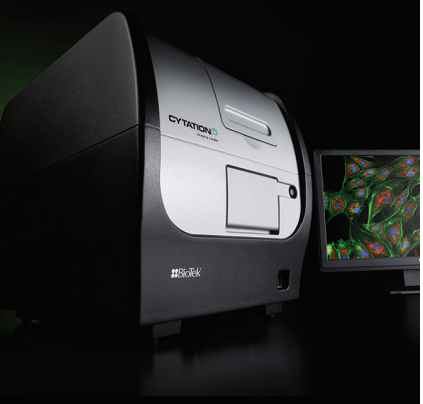

Key Words:

3D
Wound Healing
Label-Free
Cell Migration
Skin
Fibroblast
Keratinocyte
HT-1080
Brightfield Imaging

Introduction

Wound healing, both acute and chronic, involves a complex internal and external choreography of signaling, in addition to interactions with neighboring cells and the surrounding environment or external stimuli, and cell migration. This synergistic relationship can also vary depending on the wound type. Therefore, characterizing the mechanisms therein is of great interest for many applications, including wound dressing, burn and ulcer healing, scar elimination, anti-aging and aesthetic cosmetics and much more. Historically, most wound healing assays use a scratch technique, where a confluent two-dimensional (2D) cell layer is mechanically injured, and cell migration is measured. Major limitations of this method are the lack of biomimetic environment, in vivo-like architecture and multi-cellular network, and as scratching methods vary, results are difficult to replicate. Newer three-dimensional (3D) methods allow cells to self-aggregate in the absence of a solid substrate. Vital cell-cell and cell-extracellular matrix (ECM) communication networks are able to be reestablished. In this way, both cellular morphology and behavior more closely mimic that found in the body.

Here, we demonstrate a novel 3D wound healing assay model (Figure 1) that can overcome 2D assay limitations. The method incorporates magnetic levitation where cells are first incubated with a nontoxic, magnetic nanoparticle assembly consisting of gold, iron oxide and poly-L-lysine, which magnetizes the cells without inducing an inflammatory cytokine response. The cells are then placed into a microplate well and levitated by placing a magnet above the well. The cells aggregate and form ECM within a few hours, the magnet is removed, and pipetting is performed to break up the aggregate, once again creating a single cell suspension. Appropriate cell numbers are then transferred to a 384-well assay plate and a ring magnet is positioned below the plate, allowing the cells to be patterned into a new 3D ring shape. Wound healing rates are determined by monitoring ring closure once the ring magnet is removed. Two individual fibroblast cell models, HT-1080 fibrosarcoma cells and primary dermal fibroblasts, were tested to compare wound healing rates between cancer cell line and primary cell models. Co-cultures containing fibroblasts and keratinocytes were also examined to ascertain whether more *in vivo*-like cell models have an effect on wound healing rates. Automated kinetic imaging was performed using a novel cell imaging multi-mode reader to track ring closure at regular intervals during the incubation period. The combination provides an easy-to-use, robust method to generate accurate and repeatable results of the effect that new test molecules have on important wound healing applications.

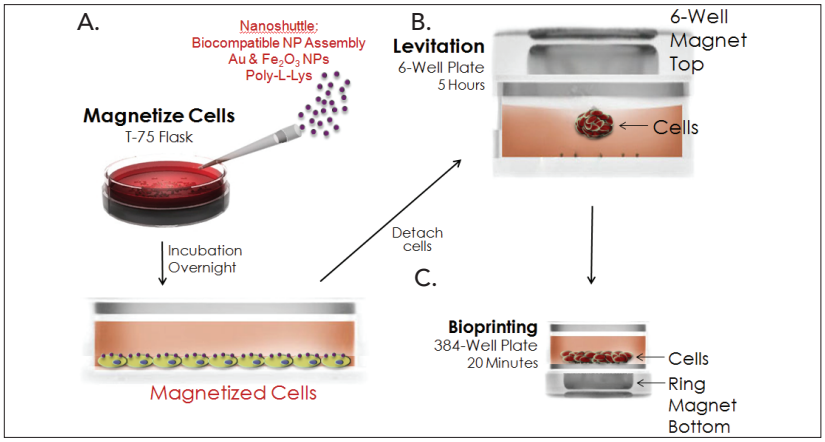

Figure 1. **BiO Assay Kit protocol.** The 384-Well BiO Assay Kit uses the NanoShuttle-PL nanoparticle assembly to (**A**) magnetize cells. After incubation, (**B**) cells are detached, resuspended in a cell-repellent plate, and magnetically levitated to aggregate and induce ECM. After breaking up the aggregates, (**C**) single cells are transferred to a 384-well cell-repellent plate placed atop a 384-well ring magnet, where they aggregate at the well bottom in the shape of the magnet. Following aggregation, the plate is removed from the magnet before placement into the imager. Cell rings will contract over time corresponding to wound healing rate of the cell model and well treatment.

BioTek Instruments, Inc.
P.O. Box 998, Highland Park,
Winooski, Vermont 05404-0998 USA
Phone: 888-451-5171
Outside the USA: 802-655-4740
Email: **customercare@biotek.com**
www.biotek.com

Materials and Methods

Materials

Assay and Experimental Components

The 384-Well BiO Assay™ Kit (GBO Catalog No. 781846, consisting of 2 vials NanoShuttle™-PL, 6-Well Levitating Magnet Drive, 384-Well Spheroid and Holding Magnet Drives (2), 96-Well Deep Well Mixing Plate, 6-Well and 384-Well Clear Cell Repellent Surface Microplates), prototype 384 well Ring Drive, and additional Cell Repellent Surface 6-Well (GBO Catalog No. 657860) and 384-Well Black µClear. Microplates (GBO Catalog No. 781976), were generously donated by Nano3D Biosciences, Inc., (Houston, TX) and Greiner Bio-One, Inc., (Monroe, NC).

The known inhibitor Cytochalasin D (Catalog No. 1233) was purchased from R&D Systems (Minneapolis, MN).

Cells

HT-1080 fibrosarcoma cells (Catalog No. CCL-121) and immortalized keratinocytes (Catalog No. CRL-2309) were obtained from ATCC (Manassas, VA). RFP expressing human neonatal dermal fibroblasts (Catalog No. cAP-0008RFP) were obtained from Angio-Proteomie (Boston, MA).

Cytation™ 5 Cell Imaging Multi-Mode Reader

Cytation 5 is a modular multi-mode microplate reader combined with automated digital microscopy. Filter- and monochromator-based microplate reading are available, and the microscopy module provides up to 60x magnification in fluorescence, brightfield, color brightfield and phase contrast. With special emphasis on live-cell assays, Cytation 5 features temperature control to 65 °C, CO_2/O_2 gas control and dual injectors for kinetic assays, and is controlled by integrated Gen5™ Data Analysis Software. The instrument performed kinetic imaging of the 3D cell structure using brightfield and red fluorescent protein (RFP) imaging channels, and a 2x objective.

Methods

Assay Procedure

T-75 flasks of cell cultures or co-cultures were cultured to 80% confluence, then treated with 600 µL NanoShuttle-PL overnight at 37 °C/5% CO_2. After incubation, cells were trypsinized, washed, and incubated for 3-5 minutes at 37 °C/5% CO_2. Cells were removed from the flasks and added to the 6-well cell repellent plate at a concentration of $1.2x10^6$ cells/well. A 6-well magnet was placed atop the well plate to levitate the cells, where they aggregated into 3D structures and induced ECM formation during a five-hour incubation at 37 °C/5% CO_2. After incubation, the cells and ECM were broken up, resuspended and added to 384-well cell repellent plate wells at a total concentration of $1.0x10^5$ cells/well, in a volume of 37.5 µL, along with 12.5 µL of 4x cytochalasin D, for a final 1x concentration of 10-0 µM. For tests involving co-cultured fibroblasts and keratinocytes, $5.0x10^4$ cells from each cell type were added to the well to create the $1.0x10^5$ total cell number. A 384-well ring magnet was placed below the well plate, and the assembly was incubated at 37 °C/5% CO_2 for 20 minutes to allow cells to aggregate into the magnet's ring shape. Following the completion of the aggregation process, the plate was removed from the ring magnet and placed into the Cytation 5. Automated brightfield imaging, using a 2x objective, captured ring closure on all wells every 30 minutes for 16 hours. Automated fluorescence imaging, using the RFP channel, was also performed on wells containing primary fibroblasts as they constitutively express RFP.

Results and Discussion

Label-Free Image-Based 3D Wound Healing Monitoring

Following the assay protocol, 100,000 total HT-1080 cells/well, were added to the 384-well cell repellent plate where kinetic brightfield imaging was performed. As illustrated by the lack of ring structure change over time (Figures 2A-B), cytochalasin D inhibits HT-1080 wound healing. Conversely, Figures 3A-E illustrate that the HT-1080 cellular ring contracts in an uninhibited setting, as seen during *in vitro* wound healing, and also demonstrates Cytation 5's ability to track uninhibited cellular ring movement throughout the entire incubation.

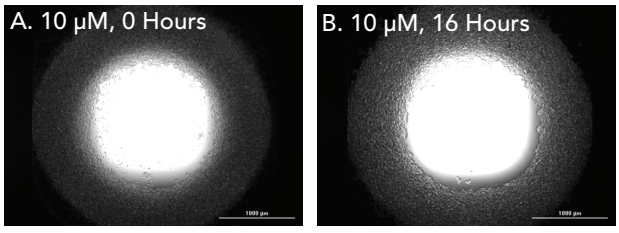

Figure 2. **HT-1080 cells treated with cytochalasin D.** 2x brightfield images captured from individual wells of HT-1080 cells treated and incubated as follows: (**A**) 10 µM cytochalasin D, 0 hours incubation; (**B**) 10 µM cytochalasin D, 16 hours incubation.

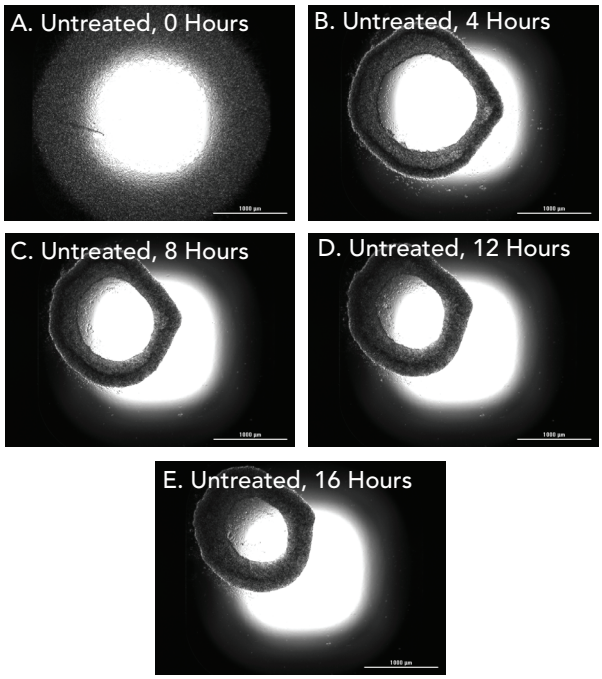

Figure 3. **Untreated (0 µM cytochalasin D) HT-1080 cells.** 2x brightfield images captured from individual wells of untreated HT-1080 cells incubated for **(A)** 0 hours; **(B)** 4 hours; **(C)** 8 hours; **(D)** 12 hours; **(E)** 16 hours.

Next, wound healing extent was analyzed using Cytation 5's brightfield imaging. Using the parameters in Table 1, object masks were automatically placed around 3D cellular structures (Figure 4) to track parameters such as object size, area and total brightfield signal over the total incubation time. As seen in the images from Figure 3 and 4, the ring structures begin as large objects and then close over time in response to the combined forces pulling on each individual cell. In order for the cell analysis algorithms of the Gen5 software to properly identify each ring as a single object, certain adjustments are necessary. Minimum and maximum object size are increased to encompass the smallest and largest ring structures. "Split touching objects" is unchecked and "Include edge objects" is checked to further enhance object identification. Finally, due to large object size, the advanced "Background flattening size" parameter is also dramatically increased. This ensures that the image information remains for proper identification of rings that can be over 2000 µm in size. In addition, because of the use of brightfield imaging and slight variations in intensity throughout the ring structure, "Image smoothing strength" is set to a high value. This and the background flattening size setting also aid in the identification of accurate single objects per well. Taken together each analysis parameter allows the identified signal threshold value to consistently place object masks around the ring, particularly when only subtle differences exist between background and ring intensity levels. It is important to note that cellular analysis parameters may vary depending on cell type. Optimization of parameters should always be performed when working with untested cell models. Object area was used for all analyses.

Brightfield Primary Cellular Analysis Parameters	
Threshold	16,000
Min. Object Size	500 µm
Max. Object Size	3,000 µm
Bright objects on a dark background	Unchecked
Split touching objects	Unchecked
Include Edge Objects	Checked
Advanced Options	
Evaluate Background On	20% of Lowest Pixels
Image Smoothing Strength	10
Background Flattening Size	10,000 µm

Table 1. **Gen5 brightfield cellular analysis parameters.** As cell types vary, parameter optimization should always be performed with untested cell models.

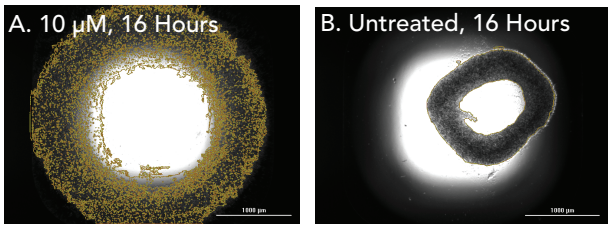

Figure 4. **HT-1080 cellular analysis using Cytation 5 2x brightfield imaging.** Object masks shown on cells treated and incubated as: **(A)** 10 µM cytochalasin D, 16 hour incubation; **(B)** 0 µM cytochalasin D (untreated), 16 hour incubation.

Finally, Cytation 5 calculated the HT-1080 3D cell ring structure's total area for each 30-minute time point, for real-time wound healing analysis. The percent of initial area decreases with time as lower cytochalasin D concentrations are added to the well. Data normalization was carried out by comparing total area at each time point to initial area (Figure 5). Additionally, per Figure 6, Cytation 5 can be used to calculate cytochalasin D IC_{50} values using single time point data.

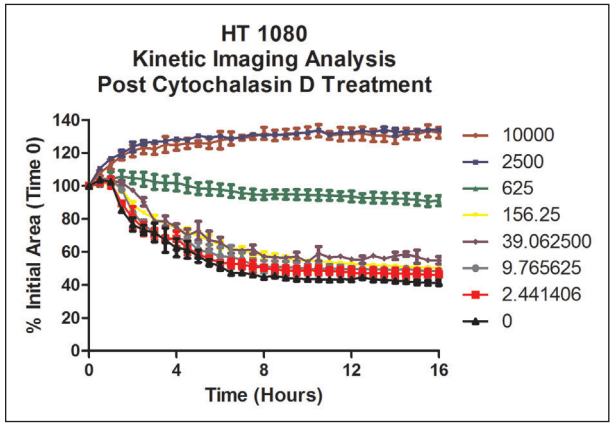

Figure 5. **HT-1080 wound healing analysis using dose-dependent percent of initial area.** Values represent nM Cytochalasin D concentrations tested per well.

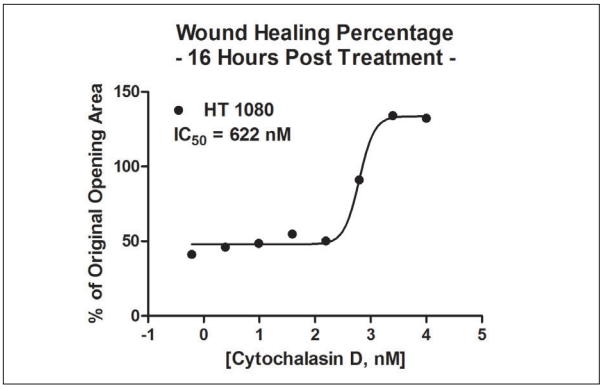

Figure 6. HT-1080 post incubation wound healing IC_{50} calculation.

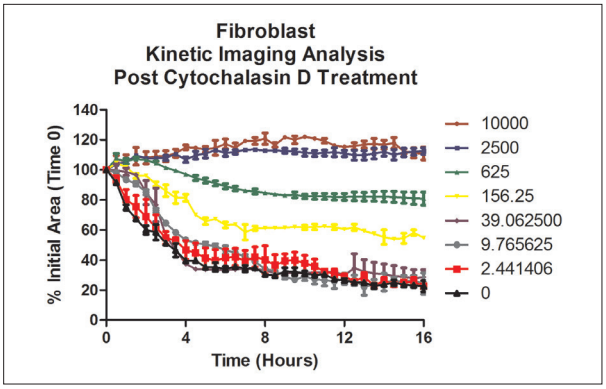

Figure 8. Kinetic primary fibroblast wound healing analysis using dose-dependent percent of initial area.

Primary Fibroblast Comparison

Using immortalized cancer cell lines as surrogate models for primary cells affords the advantage of providing a continuous cell source for experimental purposes. However, internal changes in the cancer cell may modify the migratory characteristics of the cell model as seen by Varani, *et al*. when comparing normal mouse embryo fibroblasts and mouse fibrosarcoma cells[1]. Here we tested human dermal fibroblasts using conditions previously described to examine potential differences between primary cells and the HT-1080 fibrosarcoma cell line.

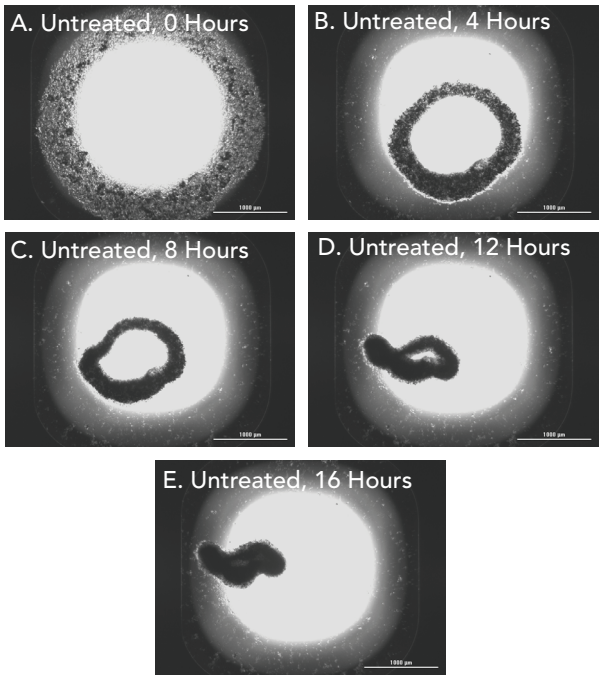

Figure 7. Untreated (0 µM cytochalasin D) primary fibroblasts cells. 2x brightfield images captured from individual wells of untreated primary fibroblast cells incubated for **(A)** 0 hours; **(B)** 4 hours; **(C)** 8 hours; **(D)** 12 hours; **(E)** 16 hours.

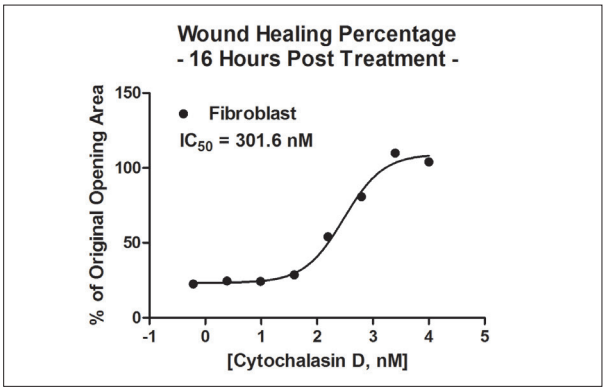

Figure 9. Primary fibroblast wound healing IC_{50} calculation.

Cytation 5 was again used to calculate the 3D cell ring total area, created using primary fibroblasts, for wells at each 30-minute time point. A greater percentage of wound healing was seen using primary cells compared to the cancer cell line. Cytochalasin D IC_{50} values, using the primary fibroblasts, were calculated (Figure 9) and demonstrated a left shift when compared to values generated with the cancer cell line.

Wound healing analysis can also be performed using Cytation 5's fluorescent imaging channels for cells labeled with a fluorescent probe or that constitutively express a fluorescent protein, such as the RFP expressing primary fibroblasts used here. Automated object masks from Table 2 were utilized to track changes in the 3D cell ring area (Figure 10). Note that the enhanced contrast provided by fluorescence relative to brightfield microscopy allowed the use of lower threshold and less aggressive background adjustment and smoothing analysis parameters. Additionally, equivalencies were seen when comparing kinetic wound healing patterns (Figure 11) and cytochalasin D IC_{50} values (Figure 12) from brightfield and RFP signals.

RFP Primary Cellular Analysis Parameters	
Threshold	5,000 RFU
Min. Object Size	500 µm
Max. Object Size	3,000 µm
Bright objects on a dark background	Checked
Split touching objects	Unchecked
Include Edge Objects	Checked
Advanced Options	
Evaluate Background On	5% of Lowest Pixels
Image Smoothing Strength	3
Background Flattening Size	Auto

Table 2. **Gen5 RFP cellular analysis parameters.** As cell types vary, parameter optimization should always be performed with untested cell models.

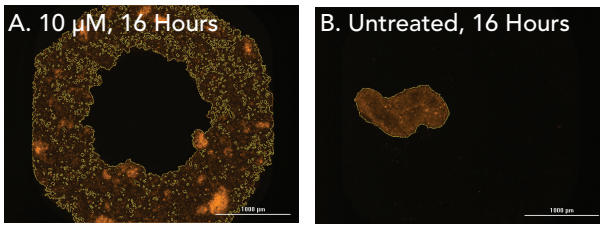

Figure 10. **Primary fibroblast cellular analysis using Cytation 5 2x RFP imaging.** Object masks shown on cells treated and incubated as: (A) 10 µM cytochalasin, 16 hour incubation; (B) 0 µM cytochalasin (untreated), 16 hour incubation.

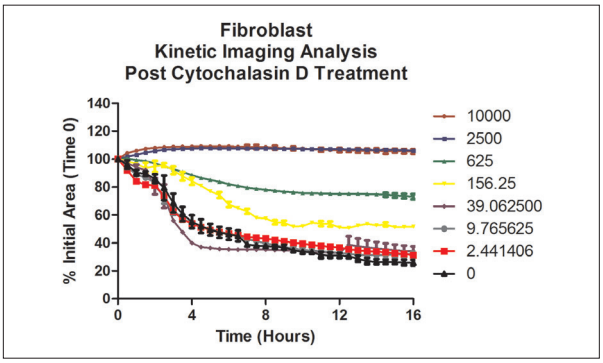

Figure 11. Kinetic primary fibroblast wound healing using RFP channel cellular analysis per cytochalasin D concentration treatment.

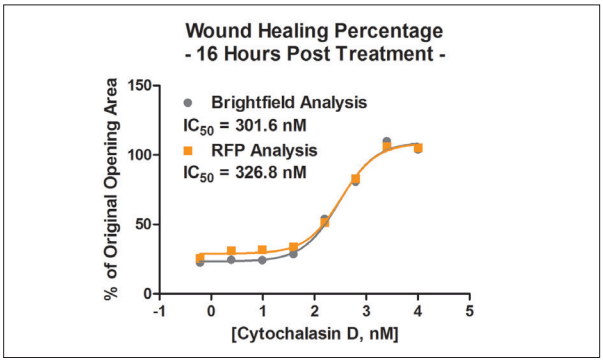

Figure 12. Comparison of primary fibroblast brightfield and RFP IC_{50} calculations.

Fibroblast and Keratinocyte Co-Culture Analysis

Finally, co-cultured wound healing was examined. Werner, *et al.* demonstrated that interactions between keratinocytes and fibroblasts dominate many phases of the wound healing process[2]. Therefore, incorporation of a co-culture of these two cell types, as shown below, may provide a more accurate representation of *in vivo* wound healing.

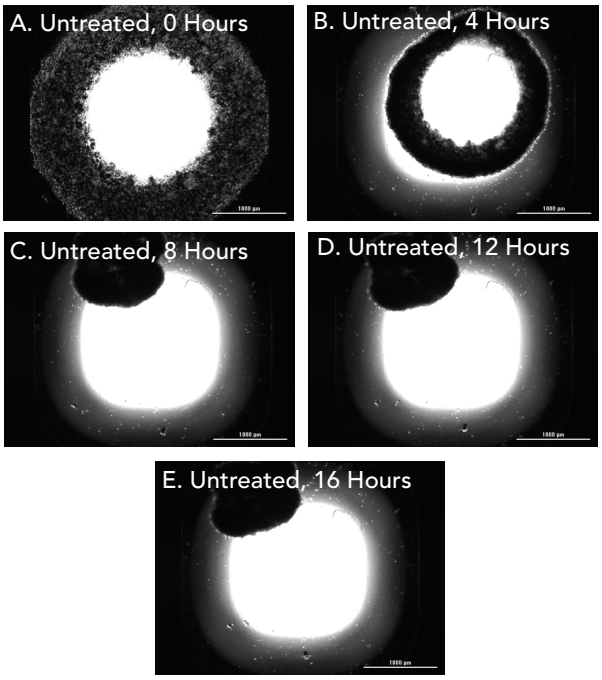

Figure 13. **Untreated (0 µM cytochalasin) primary fibroblasts and keratinocytes.** 2x brightfield images captured from individual wells of untreated co-culture incubated for (A) 0 hours; (B) 4 hours; (C) 8 hours; (D) 12 hours; (E) 16 hours.

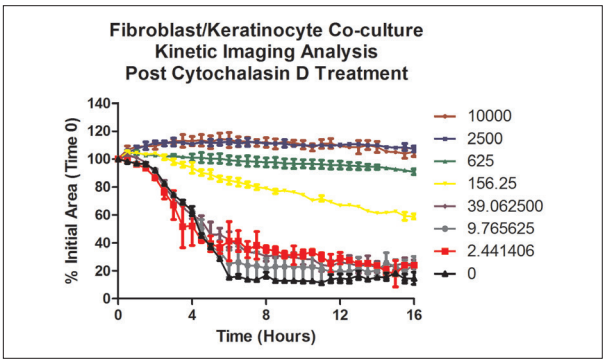

Figure 14. Kinetic co-culture wound healing analysis using cytochalasin D dose-dependent percent of initial area.

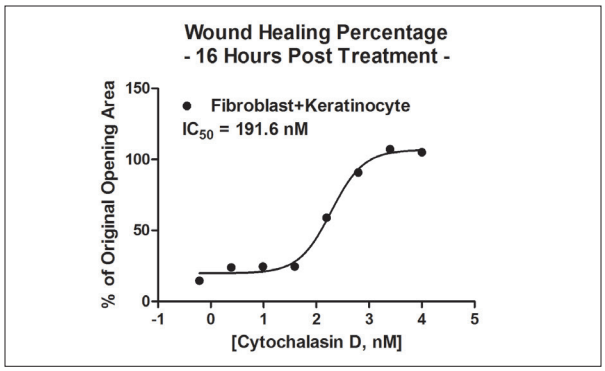

Figure 15. Co-culture post incubation wound healing IC_{50} calculation.

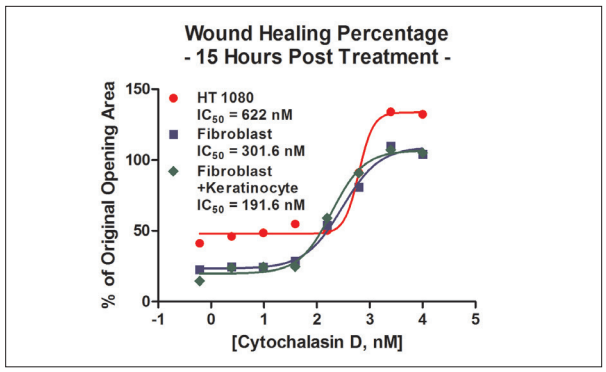

Figure 18. Wound healing IC_{50} cell model comparison.

Figures 13 and 16, and Figure 17's graph of uninhibited wound healing for all cell models, demonstrate that the fibroblast/keratinocyte co-culture increased wound healing rates compared to fibroblasts alone or cancer cells. The co-cultured 3D ring completely closes by the seventh hour, compared to moderate closure with the remaining cell models. Additionally, the HT-1080 IC50 curve was distinctly different from the other cell models, as seen in Figure 18. The cancer cell line demonstrates an extremely sleep inhibittory curve and significantly less wound healing than the other two cell models.These results validate the need for inclusion of appropriate cell models when performing wound healing analyses.

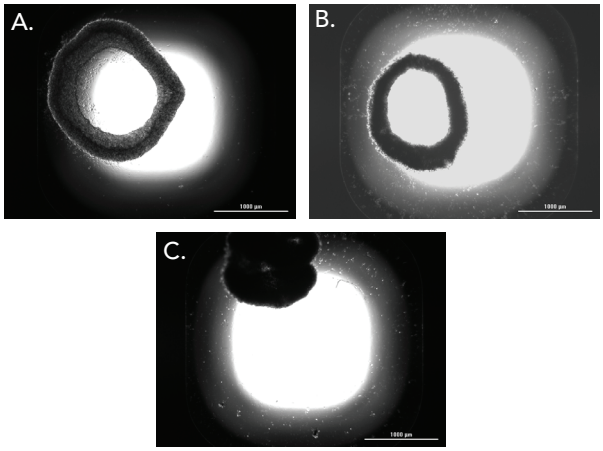

Figure 16. **Comparison of cell model wound healing.** 2x images captured from untreated **(A)** HT-1080 cells; **(B)** primary fibroblasts; **(C)** co-cultured fibroblasts and keratinocytes; each incubated for 7 hours.

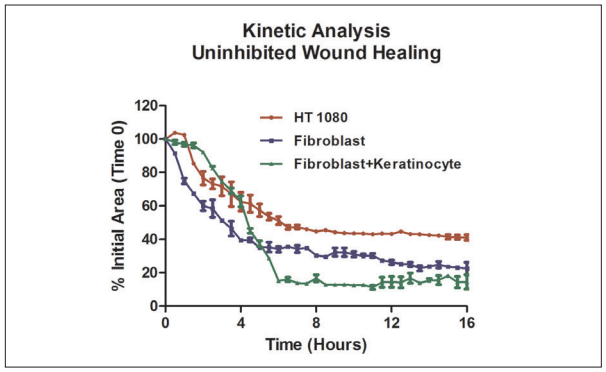

Figure 17. Wound healing rate cell model comparison.

Conclusions

The 384-Well BiO Assay Kit and NanoShuttle-PL particles from nano3D Biosciences provide a simple, robust method to carry out 3D wound healing assessments, while incorporation of Greiner Bio-One Cell-Repellent Surface 6-Well and 384-Well Microplates allow efficient cell levitation for ECM creation, and high throughput performance of the 3D wound healing assay. The addition of Cytation™ 5, with automated imaging and analysis in brightfield and fluorescence imaging channels, simplifies the assay process and increases analysis accuracy by removing manual determinations.

At the same time, use of primary cells may lead to a better understanding of *in vivo* dermal wound healing compared to cancer cells, and use of appropriate cell models, including primary and co-cultured cells, may affect the extent and rate of wound healing, in addition to sensitivity to test molecules. The combination of assay method and automated imaging and analysis creates an easy to use, robust method to generate accurate and repeatable results when used for important dermal wound healing applications.

References

1. Varani, J.; Orr, W.; Ward, P.A. A comparison of the migration patterns of normal and malignant cells in two assay systems. *Am J Pathol.* **1978**, *90*(1), 159-171.

2. Werner, S.; Krieg, T.; Smola, H. Keratinocyte-fibroblast interactions in wound healing. *J Invest Dermatol.* **2007**, *127*(5), 998-1008.